Detection and Analysis of Irregular Streaks in Dermoscopic Images of Skin Lesions

Maryam Sadeghi, *Member, IEEE*, Tim K. Lee*, *Member, IEEE*, David McLean, Harvey Lui, and M. Stella Atkins

***Abstract*—Irregular streaks are important clues for Melanoma (a potentially fatal form of skin cancer) diagnosis using dermoscopy images. This paper extends our previous algorithm to identify the absence or presence of streaks in a skin lesions, by further analyzing the appearance of detected streak lines, and performing a three-way classification for streaks, *Absent*, *Regular*, and *Irregular*, in a pigmented skin lesion. In addition, the directional pattern of detected lines is analyzed to extract their orientation features in order to detect the underlying pattern. The method uses a graphical representation to model the geometric pattern of valid streaks and the distribution and coverage of the structure. Using these proposed features of the valid streaks along with the color and texture features of the entire lesion, an accuracy of 76.1% and weighted average area under ROC curve (AUC) of 85% is achieved for classifying dermoscopy images into streaks *Absent*, *Regular*, or *Irregular* on 945 images compiled from atlases and the internet without any exclusion criteria. This challenging dataset is the largest validation dataset for streaks detection and classification published to date. The data set has also been applied to the two-class sub-problems of *Absent*/*Present* classification (accuracy of 78.3% with AUC of 83.2%) and to *Regular*/*Irregular* classification (accuracy 83.6% with AUC of 88.9%). When the method was tested on a cleaned subset of 300 images randomly selected from the 945 images, the AUC increased to 91.8%, 93.2% and 90.9% for the *Absent*/*Regular*/*Irregular*, *Absent*/*Present*, and *Regular*/*Irregular* problems, respectively.**

***Index Terms*—Computer-aided diagnosis, dermoscopic structures, dermoscopy, graph, irregular streaks, melanoma, skin cancer, streak detection, texture analysis.**

I. Introduction

MALIGNANT melanoma, a form of skin cancer arising from the pigment-producing cells of the epidermis, is most treatable when the disease is diagnosed early. However, effective therapies for metastatic melanoma are lacking, and the five year survival rate is only 15% for the advanced stage [1]. In conjunction with the fact that the incidence of the disease has been increasing rapidly and steadily in the last 30 years [2], there is an urgent need for early detection tools.

A popular *in vivo* noninvasive imaging tool among dermatologists is dermoscopy, also known as epiluminescence microscopy [3]–[5]. Specially trained dermatologists, dermoscopists, can use the tool to examine pigmented skin lesions based on a set of complex visual patterns, such as streaks, pigmented networks, blue white veil, dots, and globules [6]. According to the presence, absence and the degree of irregularity of these visual patterns, a diagnosis can be derived by following one of the dermoscopic algorithms [3], [5], [7]–[9].

Streaks, one of the important visual features, can be considered interchangeably with radial streaming or pseudopods because of the same histopathological correlation [10]. Radial streaming is a linear extension of pigment at the periphery of a lesion as radially arranged linear structures in the growth direction, and pseudopods represent finger-like projections of dark pigment (brown to black) at the periphery of the lesion [10]. Fig. 1(a) shows an example of a lesion with the radial streaming pattern, enlarged in Fig. 1(b). Fig. 1(c) shows an example of a lesion with the pseudopods pattern. The enlarged image is shown in Fig. 1(d). Streaks are *local* dermoscopic features of skin lesions, however when streaks appear symmetrically over the entire lesion [as seen in Fig. 1(a)], the feature is referred as a starburst pattern.

Streaks are important morphologic expressions of malignant melanoma, specifically melanoma in the radial growth phase [7], [11]. *Irregular* streaks are one of the most critical features (included in almost all of dermoscopy algorithms) that show high association with melanoma. In addition, Menzies *et al.* [7] found pseudopods to be one of the most specific features of superficial spreading melanoma which is a subset of malignant melanoma. Furthermore, symmetric streaks (starburst pattern) are one of the specific dermoscopic criteria to differentiate usually benign Spitz nevi (a dark nevus common in children) from melanoma, thus increasing diagnostic accuracy for pigmented Spitz nevi from 56% to 93% [12]. However, all lesions in adults exhibiting a starburst pattern should be excised for histopathological evaluation [7]. Fig. 2 shows lesions with *Absent*, *Regular*, and *Irregular* streaks.

Based on the clinical definitions in [3] *Irregular* streaks are never distributed regularly or symmetrically around the lesion. They also should not be clearly attached to pigment network lines. These definitions are used later in the paper to define discriminative models towards automated *Regular*/*Irregular* classifications of streaks.

Manuscript received November 05, 2012; revised December 19, 2012; accepted January 01, 2013. Date of publication January 14, 2013; date of current version April 27, 2013. The work of M. Sadeghi was supported in part by the Canadian Natural Sciences and Engineering Council (NSERC), in part by the CIHR-Skin Research Training Center, and in part by a grant from the Canadian Health Research Project (CHRP). *Asterisk indicates corresponding author.*

M. Sadeghi is with the Medical Image Analysis Lab, School of Computing Science, Simon Fraser University, BC, V5A 1S6 Canada (e-mail: msa68@sfu.ca).

*T. K. Lee is with the Cancer Control Research, BC Cancer Agency, Vancouver, BC, V5Z 1L3 Canada (e-mail: tlee@bccrc.ca).

D. McLean and H. Lui are with the Department of Dermatology and Skin Science, and Photomedicine Institute, University of British Columbia, Vancouver, BC, V6T 1Z4 Canada.

M. Stella Atkins is with the Medical Image Analysis Lab, School of Computing Science, Simon Fraser University, Burnaby, BC, V5A 1S6 Canada.

Color versions of one or more of the figures in this paper are available online at http://ieeexplore.ieee.org.

Digital Object Identifier 10.1109/TMI.2013.2239307

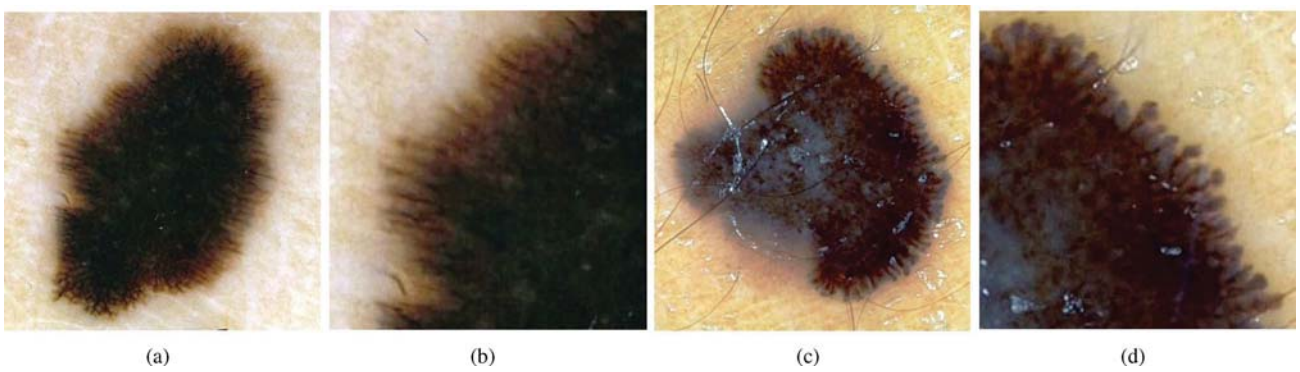

Fig. 1. Examples of streaks. Images (a) and (c) are lesions containing *radial streaming* and *pseudopods* pattern, respectively. Images (b) and (d) are magnified images to show the linear structures. Images are taken with permission from [6].

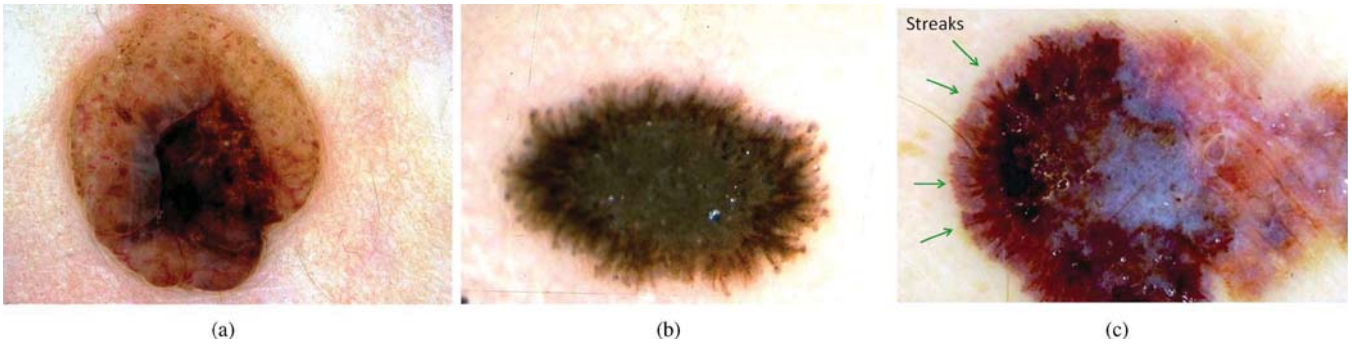

Fig. 2. Examples of *Absent*, *Regular* and *Irregular* images. Image (a) shows a lesion without streaks (*Absent*). Image (b) illustrates a lesion with a complete symmetric *Regular* streaks pattern called *starburst*, and in (c) a melanoma with *Irregular* streaks and partial distribution is shown. Images (b) and (c) are called *Present* images. Image (a) is taken from [6], (b) and (c) are from [13] with permission.

Automating the recognition of streaks would help in building a computer-aided system for melanoma detection. Such a system would not only help physicians diagnose melanoma as a second reader, it could also teach the technique of dermoscopy. This paper presents a novel automated method, which builds upon and extends the earlier work [14], [15] identifying the presence of valid streak lines from the set of candidate streak lines. This method analyzes further the orientation and spatial arrangement of streak lines and classifies the lesion as a lesion with *Absent*, *Regular*, and *Irregular* streaks.

The paper is organized as follows. Section II describes previous work on streaks analysis in dermoscopy images. Section III describes the new contributions in this paper, analyzing streak orientation, feature extraction and classification. Section IV gives details of the experiments and evaluation, and Section V presents the conclusion and future work.

II. Previous Work

As a fundamental step towards computer-aided diagnosis of skin cancers, automatic detection and analysis of local dermoscopic structures [16]–[23] and global patterns [24]–[28] have been frequently addressed in the literature. However, even though the presence of *Irregular* streaks is highly suggestive for malignancy of a lesion, the modeling, detection, and analysis of streak lines and starburst pattern have very rarely been used for automated skin lesion diagnosis. There have been only a few previous studies directly on streak detection. Fleming *et al.* [29] first proposed and outlined a method to detect streaks; they argued that the presence and absence of radial streaming and pseudopods and their characteristics could be tested from a skeleton of the pigment network. However, they did not publish the details of their algorithm. Betta *et al.* [30] developed a method in which streaks were detected by simultaneously looking for occurrence of finger-like tracks along the contour of a lesion, and brown pigmentation for the corresponding region. Dividing an image into 16 sub-images, they computed, in each sub-image, the irregularity of the lesion border and also the hue component of the original color image in the HSV color space [31]. The final diagnostic decision was made by a simple threshold on these computed values. Also in a recent work, Mirzaalian *et al.* [32] combined a physics-based flux model and machine-learning approach to classify streaks in dermoscopic images. Although the methodology is interesting, it has been tested on only 99 dermoscopic images with wide exclusion criteria.

Our previous method for detecting the presence and absence of streaks [14], [15] was tested on a large database of 300 skin lesions. Because this paper's algorithm to classify a lesion into *Absent*, *Regular*, and *Irregular* is an extension of our previous work [14], the previous algorithm which utilizes a fingerprint recognition model is briefly outlined here.

The algorithm to locate streak lines is divided into four steps: preprocessing, blob detection, feature selection, and two-class classification. In the preprocessing step, lesions are segmented using the Wighton *et al.* method [33]. Then lesions are oriented with the major axis parallel to the x-axis and their sizes are standardized. Then the RGB skin images are converted to L*a*b*, and L* is used for the rest of the analysis.

In the blob detection step, linear structures with a Gaussian cross-section profile near the border are located by four Laplacian of Gaussian (LOG) filters with different sizes, $h\text{size} = 3, 5, 7, 9$ such as

$$h(x,y) = \nabla^2[g(x,y) * f(x,y)] = [\nabla^2 g(x,y)] * f(x,y) \tag{1}$$

$$\nabla^2 g(x,y) = \left(\frac{x^2+y^2-2\sigma^2}{\sigma^4}\right)^{\frac{-(x^2+y^2)}{2\sigma^2}} \tag{2}$$

where $f(x,y)$ is the intensity value at (x,y), $g(x,y)$ is the Gaussian filter whose standard deviation σ is set to a small value of 0.1, in order to achieve high sensitivity even to a small change in intensity. 25 experiments with five different sigmas and five filter sizes were performed, and the results show that the current setting gives the best results. At the end, the union of the results from the four scales were used to form a multi-scale result.

After finding linear structures, their orientation is estimated using the averaged squared gradient flow (ASGF) algorithm [34], a technique commonly used in fingerprint detection. A squared gradient vector G_s at the pixel (x,y) is defined from a gradient vector $[G_x, G_y]^T$ by doubling its angle and squaring its magnitude such as

$$\begin{bmatrix} G_{s,x} \\ G_{s,y} \end{bmatrix} = \begin{bmatrix} {G_\rho}^2 \cos(2G_\theta) \\ {G_\rho}^2 \sin(2G_\theta) \end{bmatrix} = \begin{bmatrix} G_x^2 - G_y^2 \\ 2G_x G_y \end{bmatrix} \tag{3}$$

where

$$G_\rho = \sqrt{G_y^2 + G_x^2}, \quad G_\theta = \tan^{-1}(G_y, G_x). \tag{4}$$

The average directional flow for a block can be determined as

$$\begin{bmatrix} \overline{G_{s,x}} \\ \overline{G_{s,y}} \end{bmatrix} = \frac{1}{|W|} \begin{bmatrix} \sum_W G_x^2 - G_y^2 \\ \sum_W 2G_x G_y \end{bmatrix}. \tag{5}$$

For each block the reliability of the local orientation (the coherence of the squared gradients) is calculated as

$$\text{Reliability} = \frac{|\sum_W (G_{s,x}, G_{s,y})|}{\sum_W |(G_{s,x}, G_{s,y})|}. \tag{6}$$

When all squared gradient vectors inside a block are pointing in the exactly the same direction, *Reliability* is 1. On the other hand, a value 0 indicates the vectors point in random directions. *Reliability* is used to filter the gradient vectors; only those vectors with *Reliability* greater than 0.5 are kept.

The ridge frequency, the frequency of the detected linear parallel structures, is determined by rotating the block so that the ridges are vertical. The columns are projected down to find the peaks. The frequency of ridges is calculated by dividing the distance between the first and last peaks by (number of peaks—1). The candidate linear streak structures can then be enhanced by a Gabor filter tuned with the ridges frequency and orientation such as

$$g(x,y;f,\theta,\sigma) = \exp\left(-\frac{x'^2+y'^2}{2\sigma^2}\right)\cos(2\pi f x') \tag{7}$$

$$x' = x\cos\theta + y\sin\theta, \quad y' = -x\sin\theta + y\cos\theta. \tag{8}$$

Then 25 features are extracted from the candidate linear streak structures and from the lesion to be used for the two-class classification. One set of 12 features is based on properties of the detected candidate streak lines. There are three structural, six chromatic and three textural features. Another feature set contains the 13 common color and texture features of the entire lesion. These 25 features are fed to a SimpleLogistic classifier implemented by Weka. Testing the two-class algorithm for the absence and presence of streaks, using ten-fold cross-validation on 300 dermoscopic images (105 *Absent* and 195 *Present*), an accuracy of 0.85 (precision $= 0.835$ and recall $= 0.87$) was achieved. The accuracy for starburst pattern detection was 0.815.

III. Method for Three-Class Classification for Streaks Detection

The method for recognizing partial and complete radial streaming patterns builds upon and extends the earlier work [14], [15], through identification of valid streak lines from the set of candidate streak lines, to reduce false positive streaks such as hairs and skin lines. The method also extends the analysis to identify the orientation and spatial arrangement of streak lines. These novel geometric features are used to identify not only the presence of streak lines, but whether or not they are *Irregular* or *Regular*; important for melanoma diagnosis.

A. Identifying Valid Streak Lines From Candidate Streaks

Skin lesions are mainly circular in dermoscopy images, but they can be any shape. The lesion shape is generalized as an ellipse that has the same normalized second central moments as the lesion region. Two foci F_1 and F_2 are computed using the eccentricity of the ellipse. To test whether a line segment, for example the red line segment with the angle β_1 with respect to the horizontal direction and the centroid of A_1 in Fig. 3(a), is a streak or not, A_1 is connected to F_1 and F_2 and the angle between A_1F_1 and A_1F_2 is computed and its bisector line (A_1B_1) is found. It is expected that the orientation of a true streak line segment will coincide with the bisector line A_1B_1. To test such a condition, the angle between A_1B_1 and the line joining the foci F_1F_2 (α_1) is compared to the orientation angle β_1 of the line. All orientations counterclockwise from the horizontal axis are measured in the range of $[0, 2\pi]$. By comparing $|\alpha - \beta|$ to a constant threshold of $\pi/6$, nonstreak line segments are eliminated from the set of detected lines, and reliable line segments at every scale are found to form a multi-scale result to be used for feature extraction. For example, in Fig. 3(a), the line segment with centroid A_1 will be kept, but the line segment with the centroid A_2 will be removed. Reliable lines detected after orientation enhancement are shown in Fig. 3(b), and the result of valid streaks selection is illustrated in the Fig. 3(c). These valid streaks are ordered in the direction of the red arrow from 0 to 2π for feature extraction in the next step.

Based on the mathematical definitions of streaks proposed in [14], a new set of 18 features is proposed for streaks, called STR (streaks), which includes three Structural, three Geometric, six

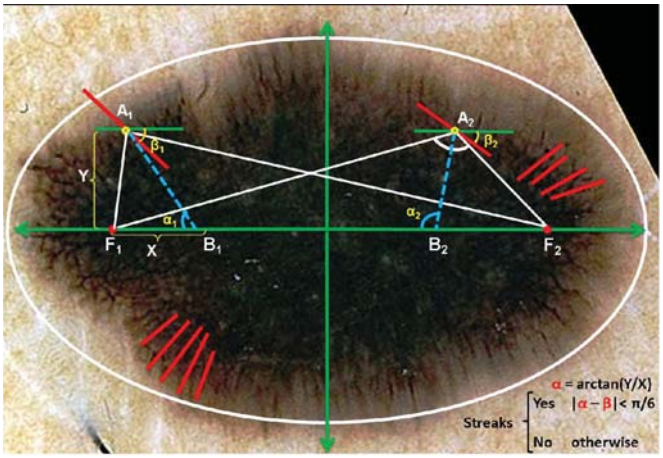

(a)

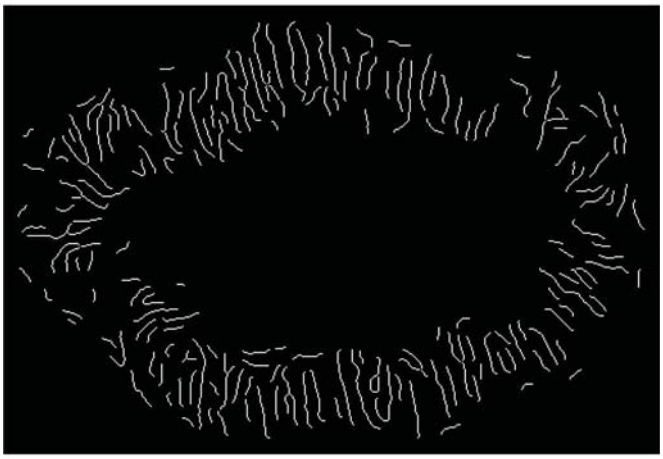

(b)

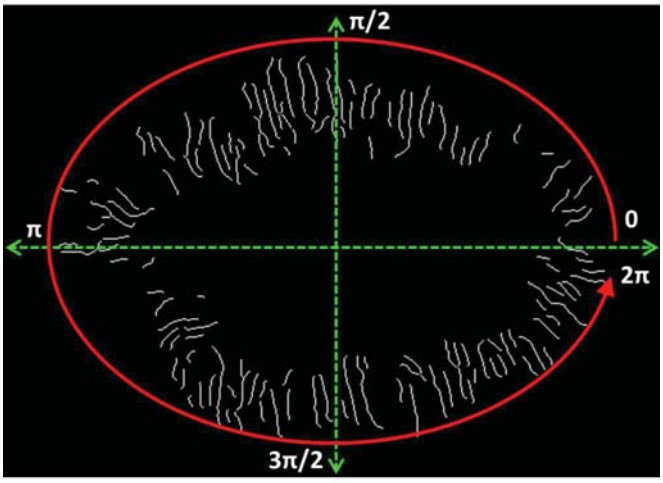

(c)

Fig. 3. Validating streaks candidates. Images (a) illustrates how line segments are filtered based on their orientation difference $(\pi/6)$ from the expected direction. Image (b) shows the line segments detected after orientation estimation and (c) shows valid streaks after removing false positives.

Orientation, and six Chromatic characteristics of valid streaks. Common color and texture features [35], [18] of the lesion itself, called LCT (lesion color texture) has also been used.

B. New STR Features

STR is a clinically inspired feature set, based on the mathematical definitions from [14] to model characteristics of *Absent*, *Regular*, and *Irregular* streaks.

1) Geometric Graph Features (Three Features): Clinically, there is an emphasis on the "uniformity" and smoothness of the orientation change in streaks for irregularity detection. There is also another important characteristic which is connectivity of the structure that represents the completeness of the pattern. In [17], Sadeghi *et al.* proposed the "Density Ratio" feature which represents the density of the dermoscopy structure called pigment network (PN). A similar concept has been used here with some modifications to measure the density of streaks on the image. This feature is useful to discriminate *Absent* images from *Present* images. For geometric analysis, a graph of the N valid streak lines found in the previous section was created by reducing each line L to v_n nodes, based on the average length of streaks in the image. For N lines, the total number of nodes equals to

$$|V| = \sum_{i=1}^{N} \left(\left(\frac{|L_i|}{\sum_{j=1}^{N} |L_j|/N} \right) + 1 \right) \tag{9}$$

where $|L_i|$ is the length of the line segment L_i in the image and $\sum_{j=1}^{N} |L_j|/N$ denotes the average length of streaks. This helps to increase the contribution of longer streak lines in feature calculation while shorter streak lines (shorter than the average length) will only have one node in the graph. Fig. 4 illustrates the node placement on streak lines based on their size to create the streak graph G. Detected streaks on a sample image are shown in Fig. 4(a) and corresponding nodes and graph lines for the green box are shown on Fig. 4(b) where the arrows point to the two streak lines longer than the average size of line segments that contribute more than one node to the graph. The white arrow points to a streak line longer than the average length, and the yellow arrow points to a streak line which is longer than two times the average length. All of the other streaks are shorter than the average length and contribute only one node each.

Density Ratio: A graph $G = (V, E)$ consists of pairs with vertices (nodes) $v \in V$ and edges $E \subseteq (V \times V)$. The standard *Density* of graph G is defined in [36] as

$$\text{Density} = \frac{2 \times |E|}{|V| \times (|V| - 1)} \tag{10}$$

which is the ratio of edges in G to the maximum possible number of edges $|E|$, and $|V|$ is the number of vertices in graph G. Inspired by [17], the density measure of the graph of streaks was defined as following:

$$\text{Density}_{\text{streaks}} = \frac{|E|(\log |E|)}{|V| \times \log(LesionSize)} \tag{11}$$

where $LesionSize$ is the size of the segmented lesion in pixels. The density feature is useful in discriminating between the *Absent* and *Present* images, however it does not say much about the regularity or irregularity of the streaks, nor the completeness and coverage of the pattern.

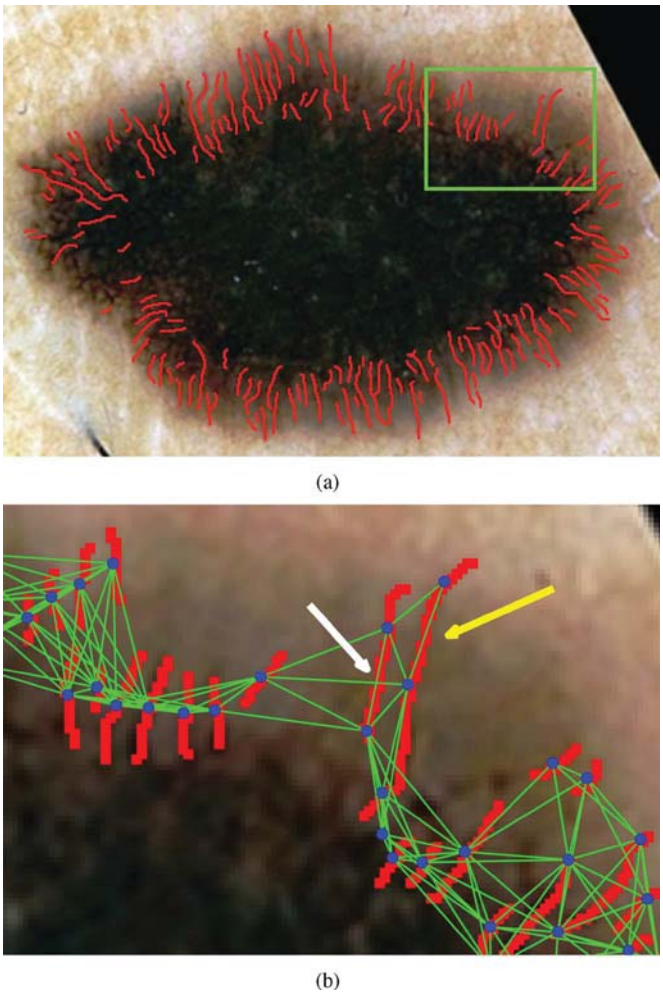

Fig. 4. Detected streaks are shown in (a) and corresponding nodes and graph lines for the green box are shown on (b) where the arrows point to the two streak lines longer than the average size of line segments that contribute more than one node to the graph. The white (left) arrow points to a streak line longer than the average length, and the yellow (right) arrow points to a streak line which is longer than two times the average length. All of the other streaks are shorter than the average length and contribute only one node each.

Often there is a complete pattern with a high graph density in *Regular* streaks all over the lesion [Fig. 5(a), (c), (e)], whereas in *Irregular* streaks, there may be a dense graph but over only small parts of the lesion [Fig. 5(b), (d), (f)]. Therefore, another measurement is needed to find out if the dense pattern is distributed all over the lesion or if it is just partially covering the lesion. Thus two new features called pattern coverage, and completeness are proposed.

Coverage: To measure the coverage of the streaks pattern, the histogram of the number of streaks in different areas (arcs) of the lesion is computed for bins of $\pi/6$ in the range of $[0, 2\pi]$. According to the mathematical definition of streaks inspired by the clinical definitions from [6], streaks are three or more linear structures co-radially oriented over the boundary of the lesion. Therefore the graph coverage was defined as the fraction of bins with more than two streak lines. Coverage ranges from 0 to 1 and the perfect coverage is equal to one that often belongs to *Regular* streaks which are distributed symmetrically among the bins [Fig. 5(g)]. Lesions with *Irregular* streaks often have a lower Coverage because of the partial distribution pattern [Fig. 5(h)]. Fig. 5(a) shows a lesion divided by red arrows into 12 areas and Fig. 5(g) shows the Coverage histogram of the lesion with *Regular* streaks. As shown in the figure, the number of streaks in the horizontal bins $\pi/6, \pi, 7\pi/6$, and 2π are often higher than other bins because of the growth pattern of the lesion in the horizontal (major) axis.

Completeness: If each vertex v_i in G is reachable from the other vertices v_j, then G is connected and a maximal connected subgraph $G_w = G(V_w, E_w)$ is the largest connected subset W of the vertex set V for which no larger set Z containing V is connected. Based on the above definitions Pattern Completeness is equal to

$$\text{Completeness} = \frac{\text{Density}_{\text{streaks}}}{|G_w|} \tag{12}$$

where $|G_w|$ is equal to the number of disconnected subgraphs (components) in the image.

2) Orientation Features (Six Features): The orientation information of valid streaks can also reveal valuable information about the presence and regularity or irregularity of streaks. The valid streaks are ordered in order to track the orientation change to detect the underlying pattern, if any. The line segments are ordered based on their location and their orientation from the major axis starting from 0 to 2π in the counter-clockwise direction [Fig. 3(c)]. In Fig. 6(a), streaks are ordered in the x axis and their corresponding orientation in the y axis are shown for a typical lesion with *Regular* streaks (in red) and a lesion with *Irregular* streaks (in green). *Regular* streaks tend to have smooth orientation changes without major jumps between consecutive data points, compared with *Irregular* streaks. After ordering the line segments, based on the fact that they should be co-radially oriented, linear regression is applied to measure the error from an expected perfect orientation change pattern, so that informative features of regularity or irregularity of the orientation change can be extracted. Assume that the ordered valid streaks x_i are indexed by the subscript i, where i ranges from 1 to N (the total number of valid streaks), and y_i is the corresponding orientation. In the linear regression, the predicted orientation y_i can be expressed as

$$\widehat{y_i} = \beta_0 + \beta_1 x_i \quad \text{for} \quad i = 1, \ldots, N \tag{13}$$

where β_0 and β_1 are the intercept and slope of the regression line. The residual, $e_i = y_i - \hat{y}_i$, is the difference between the predicted orientation of the line segment i by the model $(\widehat{y_i})$, and the true direction of line (y_i). The slope of the fitted line, β_1, is used as one of the orientation features. Fig. 6 shows also the linear regression on the orientation data of the *Regular* and *Irregular* images. The slope β_1 for the *Regular* streaks and *Irregular* streaks are 0.67 and 4.6, respectively.

The root mean square error (RMSE) of the model is calculated as (14)

$$\text{RMSE} = \sqrt{\frac{\sum_i (\widehat{y_i} - y_i)^2}{N}}. \tag{14}$$

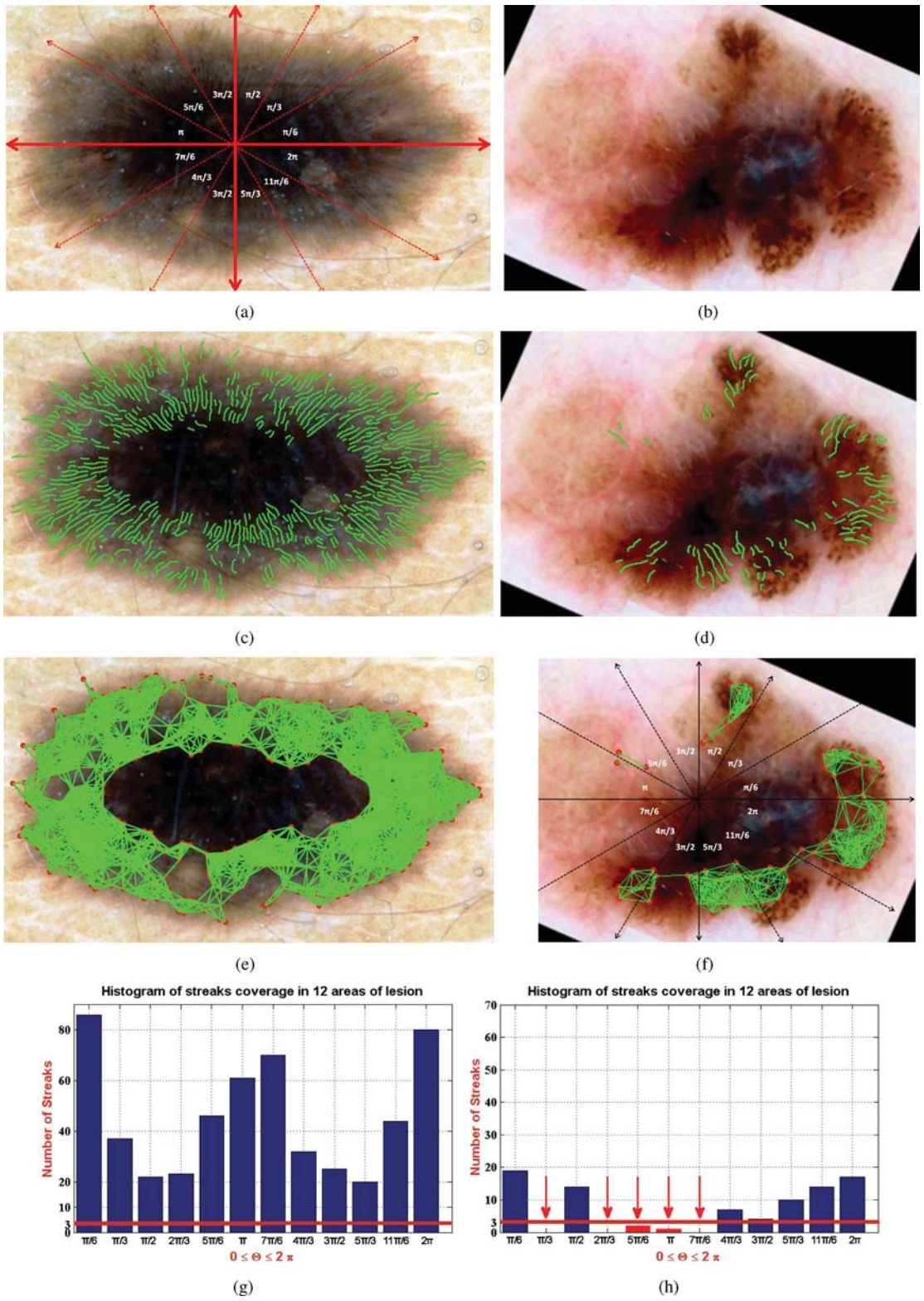

Fig. 5. Lesions with *Regular* (a) and *Irregular* (b) streaks. The red lines in (a) segment the lesion into 12 areas to calculate the coverage of streaks. (c) and (d) show the results of multi-scale streak detection on (a) and (b). (e) and (f) illustrate the graphs of streaks plotted over the lesions. In (g) and (h) the coverage histograms of (e) and (f) are shown, respectively. The histogram counts the number of streaks observations into each of the bins of $\pi/6$ in the range of $[0, 2\pi]$. From the histogram (g), Coverage is 1 (maximum) and in (h), the red arrows point to the bins with less than three line segments and Coverage is $7/12 = 0.58$.

Experiments show that images with *Regular* streaks have lower β_1 and RMSE which is because of the large number of streaks in the x axis with smooth orientation change in y. The bottom part of Fig. 6 shows the residuals of the regression corresponding to the ordered streaks above. In this example, the RMSE of the *Irregular* streaks (green plot)

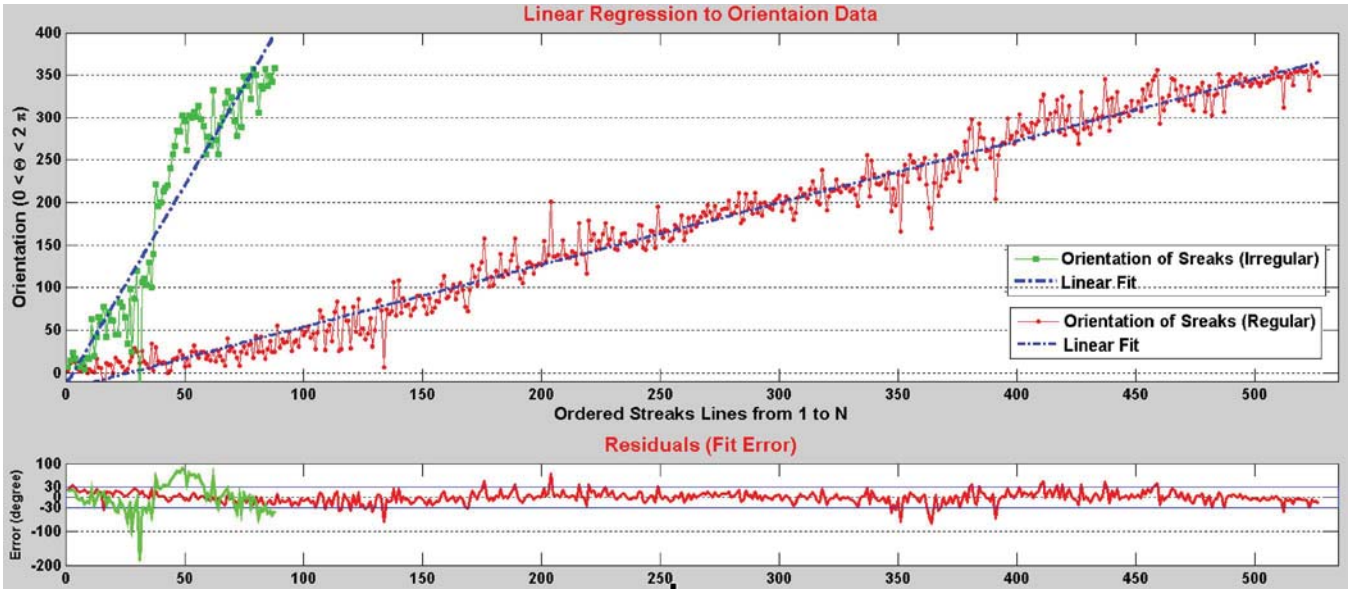

Fig. 6. Linear regression of features extracted from the orientation pattern. The top figure shows the ordered line segments in the x axis with their corresponding orientation in axis y. The red (circle) data points show the orientation data for the regular lesion shown in Fig. 5(c) and the green (square) data points illustrate the orientation of streaks of the *Irregular* lesion shown in Fig. 5(d). The bottom figure illustrates the corresponding fit error (residuals) of the linear regression. The RMSE of *Irregular* streaks (in green) is 47.68 where the RMSE error of the *Regular* streaks (in red) is 13.21. All residuals outside of the blue box in the bottom figure are counted and normalized by the number of line segments as the outliers feature.

is 47.7 and the RMSE of the *Regular* streaks (red plot) is 13.2.

Another feature involving residuals is the RMSE of the first derivative of orientations as

$$\text{RMSE\_}d = \sqrt{\frac{\sum_i (\widehat{y_i'} - y_i')^2}{N}} \tag{15}$$

where $\widehat{y'}_i$ and y_i' are the derivative of $\hat{y}_i$ and y_i.

Another is a normalized count of outlier streak lines, where outliers are defined as lines which are oriented more than $\pm 30°$ outside the defined range. These outliers can be seen outside the blue box in Fig. 6. All residuals outside of the blue box in the bottom figure are counted and normalized by the number of line segments.

The entropy of the lines orientations and residuals are also used, to characterise the randomness or existence of a specific pattern in the orientation change. The entropy is a statistical measure of randomness and the motivating idea behind the entropy is that *Irregular* streaks with unpredictable orientation change have a high entropy while *Regular* streaks with a specific smooth orientation change show a relatively low entropy. For X with N lines $\{x_i : i = 1, \ldots, N\}$, entropy is denoted by $H(X)$, and is defined as

$$H(X) = -\sum_{i=1}^{n} p(x_i) \log_b p(x_i) \tag{16}$$

where $p(x_i)$ is the probability function of x_i and contains the histogram counts of b bins where $b = (2\pi)/(\pi/18) = 36$.

3) Chromatic Features of Streaks (Six Features): The color features of streaks include the mean and standard deviation of intensity values in S and V channel of HSV color space as well as the choice of the color channel for luminance image (L* in the experiment) used for streak detection over segmented streak lines.

4) Structural Features (Three Features): Diagnostically important characteristics of streaks include the shape, length, and variability of lines. Therefore, the length of each line is computed, which is the number of pixels of the line segment. The features are the mean of the lengths of streaks, and the total number of line segments in the image. The ratio of the streak size to the lesion size (# of streak pixels/# of pixels in the lesion area) is also included.

C. Lesion Color Texture Features: LCT (13 Features)

LCT includes the following 13 features: The mean, standard deviation and reciprocal of coefficient of variation (mean/stdev) of the values in S and V from HSV and L* of L*a*b*, and four of the classical texture measures; energy, contrast, correlation, and homogeneity [37], [18]. These textural features are calculated from a grey level co-occurrence matrix (GLCM). The GLCM, constructed over the entire lesion, is a tabulation of how often different combinations of pixel brightness values (gray levels) occur in a pixel pair in an image.

The streak detection algorithm and the validation procedure outlined in the paper likely miss and/or exclude some "true" streak lines. In addition, the streak-specific features reported in Section III-B may not cover "all" streak properties. Thus the LCT feature set was constructed, in order to capture the "missing" information globally from the entire lesion. (As seen in the quantitative results in Section IV-B, combining LCT and STR features achieved the highest accuracy and confirmed our hypothesis). Potentially, the LCT set could include other dermoscopic features such as border asymmetry, irregularity and the color counts. However, the LCT set was restricted to the color and texture information that is more obviously useful for

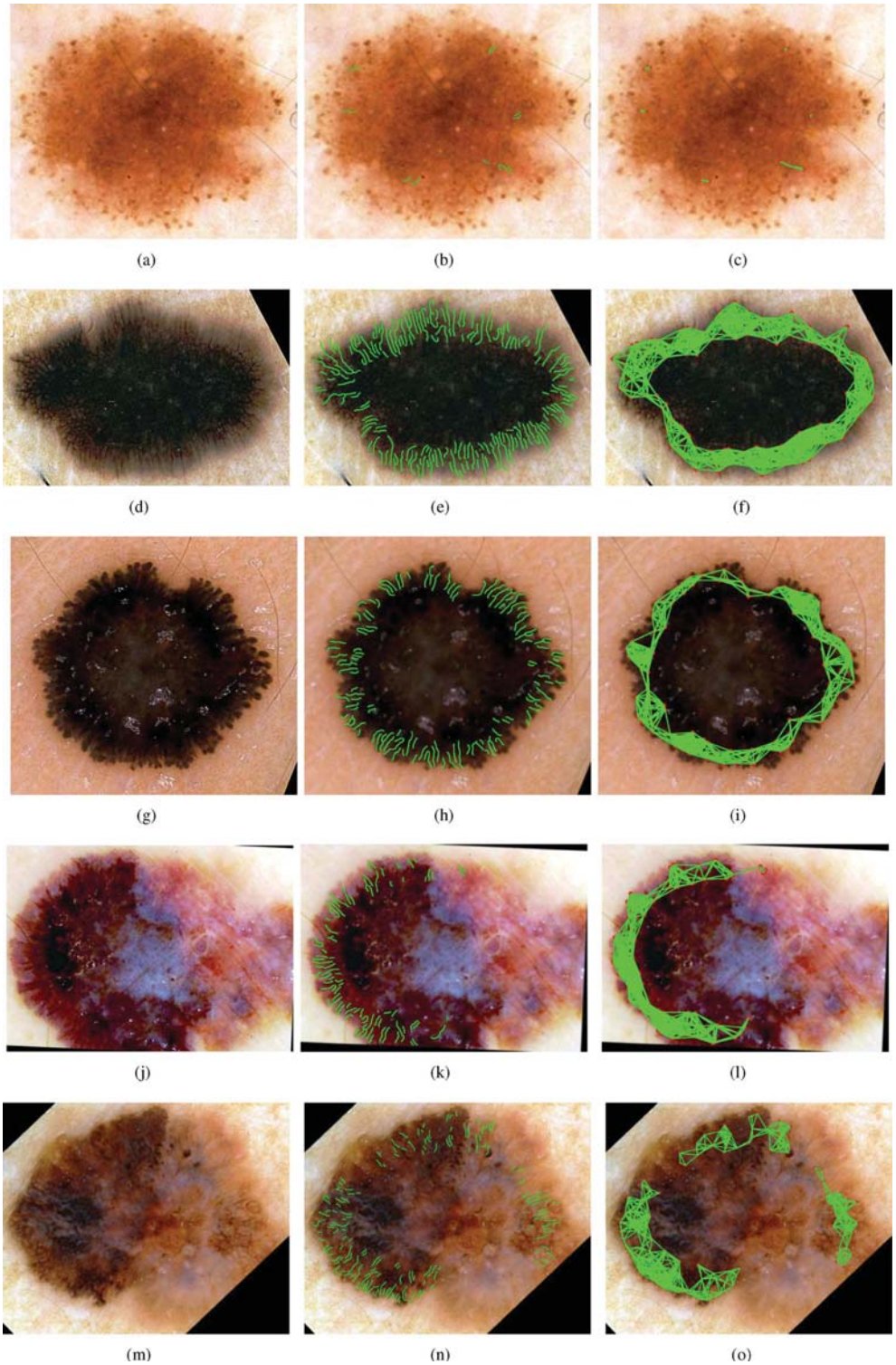

Fig. 7. Examples of each of the *Absent*, *Regular*, and *Irregular* classes are shown. (a) illustrates an *Absent* image from the experiments with streak lines and graphs in the second and third columns, respectively. (d) and (g) show two *Regular* (Spitz nevus) images with radial streaming and pseudopods, respectively, and two lesions (melanomas) with *Irregular* streaks are shown in (j) and (m).

modeling streak patterns. In future, these streak features will be compared with other dermoscopic features to determine the predictive power of each of them.

D. Classification

Finally, these 31 features are fed into the SimpleLogistic [38] classifier implemented in Weka (a general data mining tool developed by University of Waikato in New Zealand) which uses a powerful boosting algorithm, LogitBoost [39]. Boosting is a method for combining the performance of many weak features to produce a powerful classifier [39]. SimpleLogistic fits logistic models by applying LogitBoost with simple regression functions as base learners. This choice of classifier was better than others such as Logistic, and BayesNet [40].

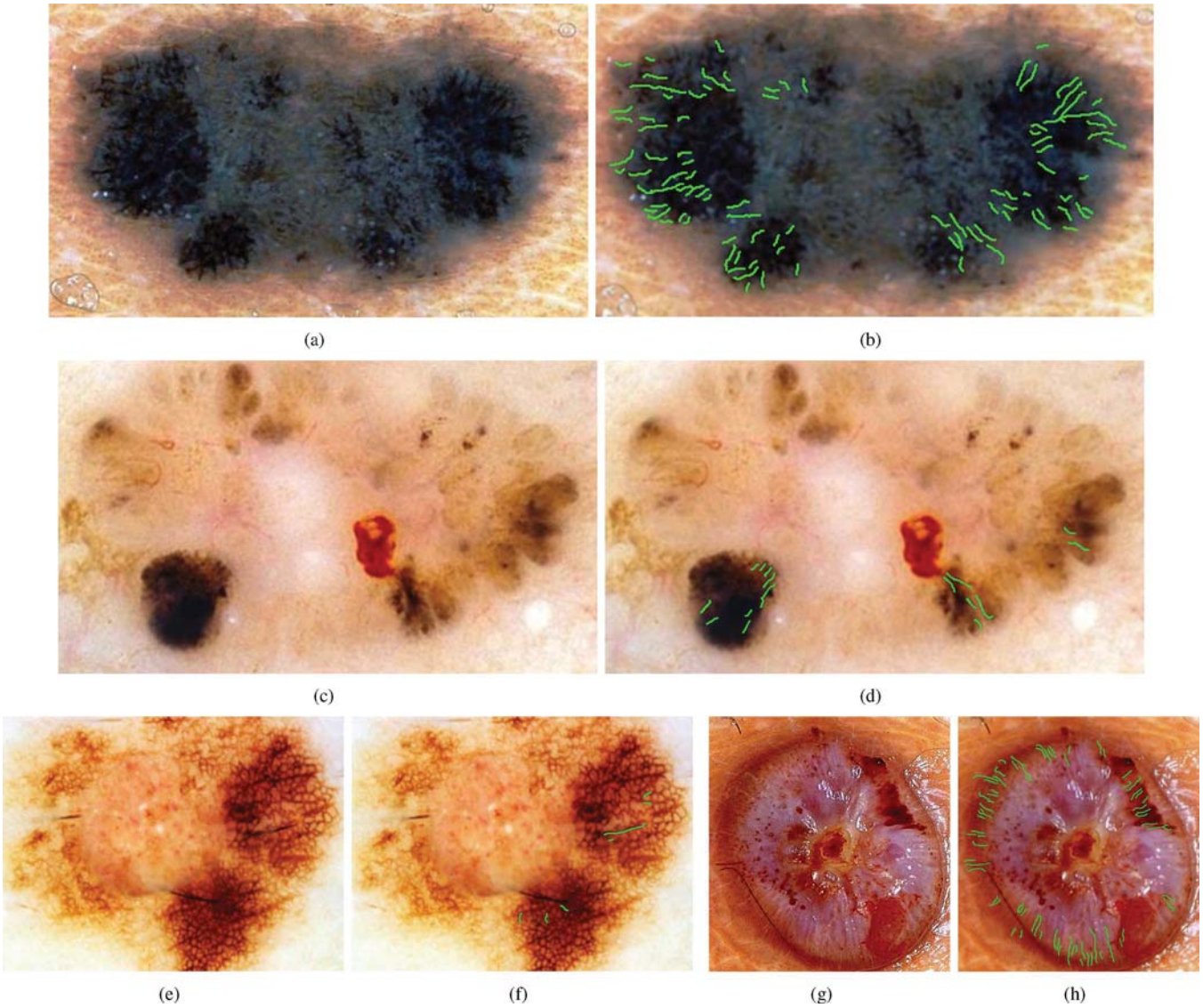

Fig. 8. Qualitative results on challenging examples. (a) shows a difficult image labeled by 40 experts with 33.3% inter-expert disagreement favoring *Present* and 26.8% disagreement favoring *Irregular* diagnosis. The method assigns a label of *Irregular* with 68% probability. Detected streak lines are shown in (b) in green. (c) shows an *Absent* image that has co-radial linear pigmented structures which belong to clods and maple leaf structures of the lesion called pigmented Basel Cell Carcinoma. A challenging lesion with a strong pigment network is shown in (e) and the result of streak detection is shown in (f) with a very few false positive lines. The method classified (c) and (e) correctly because of the low number of detected streak lines, and the low density and coverage of the graph. (g) shows one of the *Absent* images that the method failed to classify it correctly (missclassified as *Irregular*) due to the linear co-radial blood stuctures in the lesion boundary.

IV. Evaluation and Results

In the following section, results for three sets of features (LCT, STR, and LCT + STR) are reported in classifying lesions into three-classes of streaks *Absent*/*Regular*/*Irregular*, two-classes of streaks *Absent*/*Present*, and the two-classes of streaks *Regular*/*Irregular*.

In these experiments, two image sets with 945 and 300 images (a subset of the 945) were used to evaluate the proposed method. First, to evaluate the method on an inclusive image set, 945 images from different resources were used, without excluding any. Some of these images were challenging due to the acquisition parameters such as lighting and magnification, being partial (entire lesion was not visible), or due to the presence of an unreasonable amount of occlusion by either oil or hair. These challenging images are usually discarded from test sets in previous work, but we kept these images in the test set. work, but these images were kept in this test set. The method was applied to this set of 945 dermoscopic images (570 *Absent*, 245 *Irregular*, and 130 *Regular*) taken from three different resources. The first subset included 745 images from [13] where each image was labeled as (*Absent*, *Regular*, or *Irregular*) representing the presence and regularity of streaks in the image. For the second

TABLE I
Correct Classification Rates (Accuracy) of Various Image Transformations for Multi-Scale Three-Class Streaks Classification on 945 Images (Set1)

Color Channnel	G	B	Y (YIQ)	L (L*a*b)
Correct Classification	0.731	0.678	0.723	**0.761**

TABLE II
EVALUATION OF THE PROPOSED METHOD ON THE TWO SET WITH $N = 945$ (INCLUSIVE) AND $N = 300$ (SELECTED HIGH RESOLUTION AND "CLEAN") IMAGES. TWO-CLASS EXPERIMENT INCLUDES THE *ABSENT*/*PRESENT* AND *REGULAR*/*IRREGULAR* CLASSIFICATIONS AND IN THE THREE-CLASS IMAGES ARE CLASSIFIED INTO *ABSENT*/*REGULAR*/*IRREGULAR*. LCT FEATURE SET AND THE PROPOSED STR FEATURE SET HAVE BEEN EVALUATED SEPARATELY AND COMBINED. HIGHLIGHTED NUMBERS SHOW THE EVALUATION RESULTS USING ALL FEATURES $(\mathrm{LCT} + \mathrm{STR})$ COMBINED. THIS TABLE REPORTS THE SUMMARY OF THE RESULTS OF 12 EXPERIMENTS IN TERMS OF WIGHTED AVERAGE PRECISION, RECALL, F-MEASURE, ACCURACY, AND AUC FOR THE MULTI-SCALE ANALYSIS ON THE L* CHANNEL OF L*A*B*

	Experiment	N	Features	Prec.	Recall	F-Measure	Acc.	AUC
Set1	Abs/Pres	945	LCT	0.666	0.672	0.652	0.670	0.700
			STR	0.751	0.754	0.751	0.755	0.802
			LCT+STR	**0.780**	**0.782**	**0.780**	**0.783**	**0.832**
	Reg/Irr	375	LCT	0.729	0.736	0.731	0.736	0.800
			STR	0.786	0.792	0.785	0.791	0.849
			LCT+STR	**0.834**	**0.836**	**0.834**	**0.836**	**0.889**
	Abs/Reg/Irr	945	LCT	0.615	0.630	0.590	0.640	0.741
			STR	0.671	0.690	0.670	0.700	0.791
			LCT+STR	**0.744**	**0.760**	**0.742**	**0.761**	**0.850**
Set2	Abs/Pres	300	**LCT+STR**	**0.893**	**0.893**	**0.893**	**0.893**	**0.932**
	Reg/Irr	195	**LCT+STR**	**0.852**	**0.851**	**0.852**	**0.851**	**0.909**
	Abs/Reg/Irr	300	**LCT+STR**	**0.805**	**0.803**	**0.804**	**0.803**	**0.918**

subset, 100 images reported as streak *Regular* or *Irregular* were collected from the web, and for the third subset 100 images with *Absent*, *Regular*, or *Irregular* labels were taken from [6]. By adding all these three subsets, a set of 945 images (Set1) was used for the first experiment to demonstrate the strength of the proposed method over a large number of dermoscopic images from different imaging devices.

In the second experiment, a set of 300 "clean" and high resolution images were randomly selected (105 *Absent*, 110 *Irregular*, and 85 *Regular*) with a complete lesion and without artifacts such as hair or oil bubbles (Set2).

A. Evaluation-Qualitative Results

Fig. 7 illustrates five examples of qualitative results with streak lines overlaid on the images, and associated streak graphs. The first row of Fig. 7 shows an *Absent* image, with a few lines detected as potential streak lines in the second column and very sparse and low density graphs in the third column. The second and third rows illustrate results of streak detection and graphs on two images with *Regular* streaks in which Fig. 7(d) has the radial streaming streaks and Fig. 7(g) shows pseudopod streaks, demonstrating how the method successfully detects pseudopods. The last two rows of Fig. 7 show melanomas, with *Irregular* streaks. The high difference in graph densities and spatial arrangements and distribution is clear for different classes.

Streaks on dermoscopy images usually are difficult to detect since they are not perfect linear structures, but often fuzzy and low-contrast oriented intensities. Furthermore, streaks may have unpredictable spatial distribution (partial pattern) with just a few streak lines in a small region of a lesion. Therefore, it is not easy to detect them using general oriented pattern analysis. Detection and diagnosis of *Absent*, *Regular*, and *Irregular* streaks is challenging even for experts. According to [6] there was an average disagreement of 24.5% on two-class problem (*Absent*/*Present*) between 40 Experts. The difficulty and disagreement is even more on the three-class problem for detecting *Irregular* streaks. Fig. 8 shows three examples of challenging images from the difficult image set with 945 images.

Fig. 8(a) shows the result of streak detection on a difficult case [6, case 43, p. 150] that is labeled as: *Absent* (33.3%), *Regular* (17.9%), and *Irregular* (48.7%). The proposed method assigns a label of *Irregular* with 68% probability. Detected streak lines are shown in Fig. 8(b) in green. Fig. 8(c) shows an *Absent* image that has co-radial linear pigmented structures which belong to clods and maple leaf structures in a pigmented basal cell carcinoma. The method classified the image correctly because of the low number of detected streak lines and the low density and coverage of the graph. Another challenging lesion with a strong pigment network is shown in (e) and the result of streak detection is shown in (f) with a very few false positive lines in green, and correctly classified as *Absent*. Fig. 8(g) shows one of the missclassified images. It is an *Absent* image with unspecific patterns that was diagnosed to be excised, but due to the linear co-radial stuctures in the boundary area of the lesion, it is missclassified as *Irregular*.

B. Evaluation-Quantitative Results

To evaluate the generalizability of the method, a ten-fold cross-validation was conducted in the first experiment on Set1 with five scales (four scales of $h\mathrm{size}_k = 3, 5, 7, 9$ and union of these scales) in four color channels, in total 20 settings. The color channels used as the luminance image for streak detection are B and G channels of RGB, L of L*a*b*, and Y from YIQ $(Y = 0.299R + 0.587G + 0.114B)$. Table I shows the results on Set1 with 945 images, using different color transformations on the multi-scale three-class classification (*Absent*/*Regular*/*Irregular*) in which the L channel of L*a*b* outperformed the others. The best setting is used in the second experiment on Set2 with $N = 300$ images and Recall (i.e., Sensitivity, TP/(TP+FN)), Precision (i.e., Positive Predictive Value, TP/(TP+FP)), $\mathrm{Accuracy} = (\mathrm{TP} + \mathrm{TN})/N$, and AUC (the Area Under ROC Curve) are reported.

Table II summarizes the evaluation of the method for the two-class (*Absent*/*Present* and *Regular*/*Irregular*), and three-class (*Absent*/*Regular*/*Irregular*) classifications in Set1 and Set2 using different feature sets: LCT, STR, and $\mathrm{LCT} + \mathrm{STR}$. The highlighted numbers in the table show the evaluation results using all features $(\mathrm{LCT} + \mathrm{STR})$ combined.

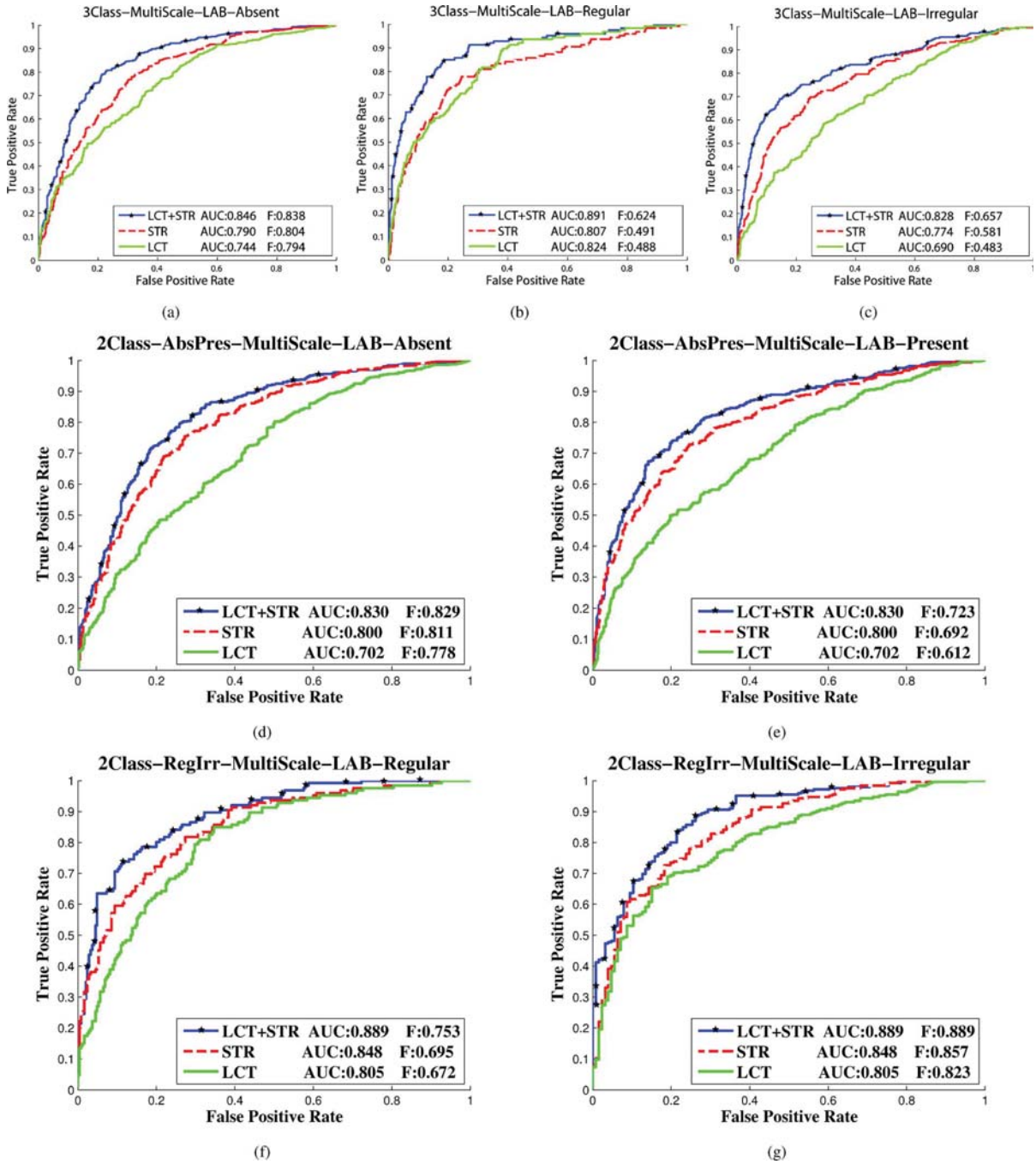

Fig. 9. ROC curves of multi-scale streak detection using the LCT, STR, and $\mathrm{LCT} + \mathrm{STR}$ feature sets in Set1 with $N = 945$ images. (a), (b), and (c) show the AUC and F-Measure of the three-class classification for the *Absent*, *Regular*, and *Irregular* classes, respectively. (d) and (e) present the performance of the approach for *Absent*/*Present* classification for the *Absent* and *Present* classes, respectively. The ROC curves on *Regular*/*Irregular* classification are shown in (f) and (g) for the *Regular* and *Irregular* classes, respectively. In all of the plots except (b), the proposed feature set STR outperforms the LCT set and using all features together $(\mathrm{STR} + \mathrm{LCT})$ results in a significant improvement in AUC and F-Measure of all classifications.

This table reports the results of 12 experiments in terms of Precision, Recall, F-measure, Accuracy and weighted average area under curve (AUC) for the multi-scale analysis on the L channel of L*a*b*. The weighted average AUC is a good performance measure in imbalanced data sets with unequal numbers of observations in each class such as Set1 because it illustrates the behavior of the classifier without regard to class distributions or error costs [41].

A ten-fold cross-validation is used to evaluate the method. As shown in Table II, by combining the new features and the common color and texture features, an accuracy of 76.1% and AUC of 85% was achieved for classifying streaks into *Absent*, *Regular*, and *Irregular*, on $N = 945$ images (Set1) without any exclusion criteria. The method was also validated on a "clean" sub-set of Set1 with $N = 300$ images with high contrast and no artifacts. The classification accuracy for the three-class problem on the second set is 80.3% with AUC of 91.8%. The method also works well on discriminating *Regular* streaks from *Irregular* ones with AUC of 88.9% on Set1 with $N = 945$ images.

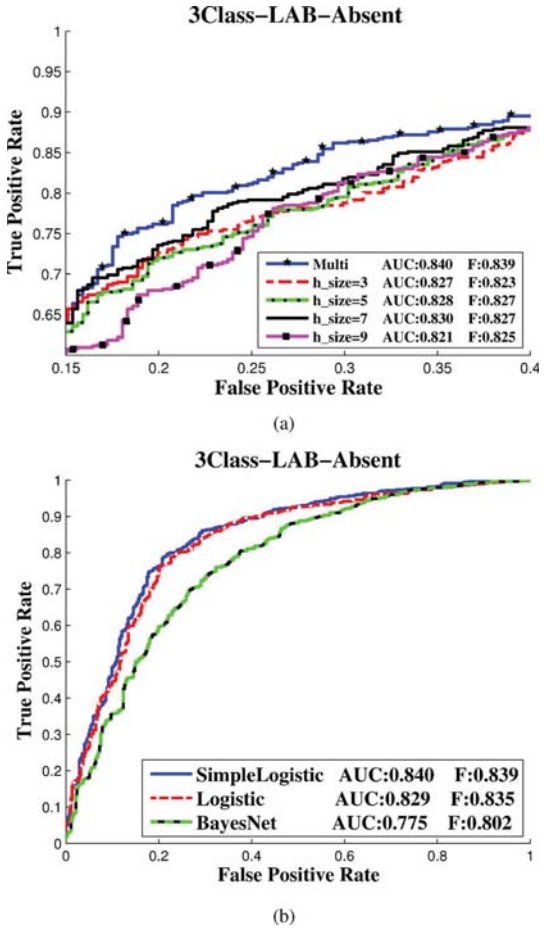

Fig. 10. ROC evaluation for different scales and classifiers. (a) shows the results of different scales ($h\text{size}_k = 3, 5, 7, 9$) and union of these scales in *Absent*/*Regular*/*Irregular* classification of streaks in the L* and (b) presents the performance of different classifiers using all features ($\text{LCT} + \text{STR}$) in the L* channel with multi-scale settings).

As mentioned before, Table II reports the weighted average of the performance measures. To show the class specific results on Set1, Figs. 9 and 10 illustrate a detailed evaluation on the three-class (*Absent*/*Regular*/*Irregular*) and the two-class (*Absent*/*Present* and *Regular*/*Irregular*) problems. Fig. 9(a), (b), and (c) show class specific results of the method in more details for the *Absent*, *Regular*, and *Irregular* classes, respectively, for Set1 with 945 images. ROC curves of classifications using STR, LCT, and $\text{STR} + \text{LCT}$ are shown to demonstrate the strength of the proposed features in discriminating between *Absent*, *Regular*, and *Irregular* streaks. Fig. 9(d) and (e) illustrates the ROC curves of *Absent* and *Present* labels in the two class problem of *Absent*/*Present* classification, and results of the *Regular*/*Irregular* classification are shown in Fig. 9(f) and (g) for the *Regular* and *Irregular* labels, respectively. In almost all of the plots [except Fig. 9(b)] the proposed feature set STR outperforms the LCT set and using all features together ($\text{STR} + \text{LCT}$) results in a significant improvement in AUC and F-Measure of all classifications.

As explained earlier, four different scales are used for streak detection ($h\text{size}_k = 3, 5, 7, 9$) and then the responses are combined to achieve the final multi-scale result. Fig. 10(a) shows the ROC curves of different scales for the class *Absent* in the three-class classification of streaks in the L* channel on Set1. The multi-scale analysis outperforms the single scales with AUC of 84%. Results of classification on Set1 using ROC curves of three different classifiers, Simple Logistic, Logistic, and Bayes Net in Figs. 10(b) have also been reported.

It is not possible to compare these results directly with previous work by others, because it is not known which images were used in their experiments. However, a difficult dataset of 945 images was deliberately created, by not excluding oily, hairy, low-contrast, and partial images to demonstrate the strength of the method. Images used in [32] are from the same source used in these experiments. Assuming the difficulty level of the images in [32] is similar to those of Set2 with 300 images, this approach achieves an AUC of 93.2% compared with 83% reported in [32] for the two-class *Absent*/*Present* classification on 99 images. Finally, the result for the two-class *Absent*/*Present* classification using Set2, is compared with our previous work [14]. Both experiments analyzed the same 300 images, but [14] uses only three STR, six chromatic features, and three texture characteristics. Results show Precision, Recall, F-Measure, Accuracy, and AUC of 0.85, 0.87, 0.86, 0.85, and 0.905 for [14] compared with 0.893, 0.893, 0.893, 0.893, and 0.932 for the current work, respectively.

V. Conclusion and Future Work

This paper has presented an automatic approach for detection of *Absent*, *Regular*, and *Irregular* streak patterns on 945 dermoscopic images, by extending our previous techniques of detecting streak line candidates [14]. Orientation estimation and correction is applied to detect low contrast and fuzzy streak lines and the detected line segments are used to extract clinically inspired feature sets for orientation analysis of the structure. A graph representation is used to analyze the geometric pattern of the structure over the lesion with new features designed to model the distribution and coverage of the structure. WThese results demonstrate that the proposed approach can locate, visualize, and classify streaks as *Absent*, *Regular*, and *Irregular* in dermoscopy images. Therefore, it can be used in computer-aided melanoma diagnosis using scoring methods. Furthermore, since the proposed method locates streaks and provides a qualitative analysis, it can be used to highlight suspicious areas for experts' diagnosis and for visualization and training purposes.

The method has been successfully applied in the specific case of automatic detection and classification of streaks, which are represented by linear radial patterns. These oriented patterns, produced by propagation, accretion, and deformation in radial phase, are common in nature and also in different fields of computer vision, and they are an important class for visual analysis. Our approach may help to understand such patterns, by analysis of co-radial linear structures in low contrast and low resolution images, in other applications such as video capsule endoscopy, mammography, iris detection in retina images, sunspot modeling, industry, and manufacturing.

The current algorithm generalizes the lesion shape to an ellipse (Section III-A). Despite the fact that many skin lesions are circular, this generalization may reduce the detection accuracy due to the fact that a skin lesion can be any shape. Also

to make sure that irregular streaks are not removed (as much as possible) in the false positive removal by orientation analysis, a threshold of 30° has been used for the difference from the desired orientation.

In future work, the segmented line segments will be investigated more locally to deal with this problem more accurately, by carefully analyzing the lesion shape and fitting multiple ellipses. In such cases, as many streaks as possible would be captured.

REFERENCES

[1] C. M. Balch *et al.*, "Final version of 2009 AJCC melanoma staging and classification," *J. Clin. Oncol.*, vol. 27, no. 36, pp. 6199–6206, 2009.

[2] Cancer facts and figures Am. Cancer Soc., 2009.

[3] H. Pehamberger, A. Steiner, and K. Wolff, "In vivo epiluminescence microscopy of pigmented skin lesions. I. Pattern analysis of pigmented skin lesions," *J. Am. Acad. Dermatol.*, vol. 17, no. 4, pp. 571–583, 1987.

[4] H. Pehamberger, M. Binder, A. Steiner, and K. Wolff, "In vivo epiluminescence microscopy: Improvement of early diagnosis of melanoma," *J. Invest. Dermatol.*, vol. 100, pp. 356S–362S, 1993.

[5] F. Nachbar, W. Stolz, T. Merkle, A. B. Cognetta, T. Vogt, M. Landthaler, P. Bilek, O. Braun-Falco, and G. Plewig, "The ABCD rule of dermatoscopy: High prospective value in the diagnosis of doubtful melanocytic skin lesions," *J. Am. Acad. Dermatol.*, vol. 30, no. 4, pp. 551–559, 1994.

[6] H. Soyer *et al.*, "Dermoscopy of pigmented skin lesions," in *An Atlas Based on the Consensus Net Meeting on Dermoscopy 2000*. Milan, Italy: Edra Medical, 2001.

[7] S. Menzies, C. Ingvar, and W. McCarthy, "A sensitivity and specificity analysis of the surface microscopy features of invasive melanoma.," *Melanoma Res.*, vol. 6, no. 1, pp. 55–62, 1996.

[8] G. Argenziano, G. Fabbrocini, P. Carli, V. De Giorgi, E. Sammarco, and M. Delfino, "Epiluminescence microscopy for the diagnosis of doubtful melanocytic skin lesions: Comparison of the ABCD rule of dermatoscopy and a new 7-point checklist based on pattern analysis," *Arch. Dermatol.*, vol. 134, no. 12, pp. 1563–1570, 1998.

[9] H. Ganster, P. Pinz, R. Rohrer, E. Wildling, M. Binder, and H. Kittler, "Automated melanoma recognition," *IEEE Trans. Med. Imag.*, vol. 20, no. 3, pp. 233–239, Mar. 2001.

[10] R. P. Braun, H. S. Rabinovitz, M. Oliviero, A. W. Kopf, and J. H. Saurat, "Dermoscopy of pigmented skin lesions," *J. Am. Acad. Dermatol.*, vol. 52, no. 1, pp. 109–121, 2005.

[11] A. Steiner, M. Binder, M. Schemper, K. Wolff, and H. Pehamberger, "Statistical evaluation of epiluminescence microscopy criteria for melanocytic pigmented skin lesions," *J. Am. Acad. Dermatol.*, vol. 29, no. 4, pp. 581–588, 1993.

[12] A. Steiner, H. Pehamberger, M. Binder, and K. Wolff, "Pigmented spitz nevi: Improvement of the diagnostic accuracy by epiluminescence microscopy," *J. Am. Acad. Dermatol.*, vol. 27, no. 5, pp. 697–701, 1992.

[13] G. Argenziano *et al., Interactive Atlas of Dermoscopy*. Milan, Italy: Edra, 2000.

[14] M. Sadeghi, T. K. Lee, D. McLean, H. Lui, and M. S. Atkins, "Oriented pattern analysis for streak detection in dermoscopy images," in *Med. Image Comput. Comput.-Assist. Intervent. (MICCAI 2012)*, 2012, pp. 298–306.

[15] M. Sadeghi, T. K. Lee, H. Lui, D. McLean, and M. S. Atkins, "Automated detection and analysis of dermoscopic structures on dermoscopy images," in *ACM Graduate Student Res. Competit. (Grace Hopper Celebration)*, 2011 [Online]. Available: http://src.acm.org/2012/MaryamSadeghi.pdf

[16] B. Shrestha *et al.*, "Detection of atypical texture features in early malignant melanoma," *Skin Res. Tech.*, vol. 16, no. 1, pp. 60–65, 2010.

[17] M. Sadeghi, M. Razmara, T. K. Lee, and M. S. Atkins, "A novel method for detection of pigment network in dermoscopic images using graphs," *Comput. Med. Imag.Graph.*, vol. 35, no. 2, pp. 137–143, 2011.

[18] M. Sadeghi, M. Razmara, P. Wighton, T. K. Lee, and M. S. Atkins, "Modeling the dermoscopic structure pigment network using a clinically inspired feature set," in *Medical Imaging and Augmented Reality*. New York: Springer, 2010, vol. 6326, Lecture Notes Comput. Sci., pp. 467–474.

[19] M. Anantha, R. H. Moss, and W. V. Stoecker, "Detection of pigment network in dermatoscopy images using texture analysis," *Comput. Med. Imag. Graph.*, vol. 28, no. 5, pp. 225–234, Jul. 2004.

[20] G. Betta *et al.*, "Dermoscopic image-analysis system: Estimation of atypical pigment network and atypical vascular pattern," in *IEEE Int. Workshop Med. Meas. Appl.*, 2006, pp. 63–67.

[21] M. E. Celebi, H. Iyatomi, W. V. Stoecker, R. H. Moss, H. S. Rabinovitz, G. Argenziano, and H. P. Soyer, "Automatic detection of blue-white veil and related structures in dermoscopy images," *Comput. Med. Imag. Graph.*, vol. 32, no. 8, p. 670, 2008.

[22] C. Barata, J. S. Marques, and J. Rozeira, "Detecting the pigment network in dermoscopy images: A directional approach," in *Proc. Int. Conf. Eng. Med. Biol. Soc.*, 2011, pp. 5120–5123.

[23] K. Korotkov and R. Garcia, "Computerized analysis of pigmented skin lesions: A review," *Artif. Intell. Med.* vol. 56, no. 2, pp. 69–90, 2012.

[24] C. Serrano and B. Acha, "Pattern analysis of dermoscopic images based on markov random fields," *Pattern Recognit.*, vol. 42, no. 6, pp. 1052–1057, 2009.

[25] T. Tanaka, S. Torii, I. Kabuta, K. Shimizu, and M. Tanaka, "Pattern classification of nevus with texture analysis," *IEEJ Trans. Elect. Electron. Eng.*, vol. 3, no. 1, pp. 143–150, 2008.

[26] Q. Abbas, M. E. Celebi, and I. Fondón, "Computer-aided pattern classification system for dermoscopy images," *Skin Res. Technol.*, vol. 18, no. 3, pp. 278–289, 2011.

[27] Q. Abbas, M. E. Celebi, and I. Fondon, "Pattern classification of dermoscopy images: A perceptually uniform model," *Pattern Recognit.*, vol. 46, no. 1, pp. 86–97, 2013.

[28] M. Sadeghi, T. K. Lee, D. McLean, H. Lui, and M. S. Atkins, "Global pattern analysis and classification of dermoscopic images using textons," in *Proc. SPIE*, 2012, vol. 8314, pp. 168–173.

[29] M. G. Fleming *et al.*, "Techniques for a structural analysis of dermatoscopic imagery," *Comput. Med. Imag. Graph.*, vol. 22, no. 5, pp. 375–389, 1998.

[30] G. Betta and G. E. Di Leo, "Automated application of the 7-point checklist diagnosis method for skin lesions: Estimation of chromatic and shape parameters," in *Proc. IEEE Instrum. Meas. Technol. Conf.*, 2005, pp. 1818–1822.

[31] T. Y. Shih, "The reversibility of six geometric color spaces," *Photogrammetric Eng. Remote Sens.*, vol. 61, no. 10, pp. 1223–1232, 1995.

[32] H. Mirzaalian, T. K. Lee, and G. Hamarneh, "Learning features for streak detection in dermoscopic color images using localized radial flux of principal intensity curvature," in *Proc. IEEE Workshop Math. Methods Biomed. Image Anal.*, 2012, pp. 97–101.

[33] P. Wighton, M. Sadeghi, T. K. Lee, and M. S. Atkins, "A fully automatic random walker segmentation for skin lesions in a supervised setting," in *Proc. MICCAI*, 2009, pp. 1108–1115.

[34] M. Kass and A. Witkin, "Analyzing oriented patterns," *Comput. Vis., Graph., Image Process.*, vol. 37, no. 3, pp. 362–385, 1987.

[35] M. E. Celebi, H. A. Kingravi, B. Uddin, H. Iyatomi, Y. A. Aslandogan, W. V. Stoecker, and R. H. Moss, "A methodological approach to the classification of dermoscopy images," *Comput. Med. Imag. Graph.*, vol. 31, no. 6, pp. 362–373, 2007.

[36] T. F. Coleman and J. J. Moré, "Estimation of sparse jacobian matrices and graph coloring problems," *SIAM J. Num. Anal.*, pp. 187–209, 1983.

[37] R. M. Haralick, I. Dinstein, and K. Shanmugam, "Textural features for image classification," *IEEE Trans. Syst., Man, Cyber.*, vol. 3, no. 6, pp. 610–621, Nov. 1973.

[38] N. Landwehr, M. Hall, and E. Frank, "Logistic model trees," *Mach. Learn.*, vol. 59, no. 1, pp. 161–205, 2005.

[39] J. Friedman, T. Hastie, and R. Tibshirani, "Additive logistic regression: A statistical view of boosting (with discussion and a rejoinder by the authors)," *Ann. Stat.*, vol. 28, no. 2, pp. 337–407, 2000.

[40] N. Friedman, D. Geiger, and M. Goldszmidt, "Bayesian network classifiers," *Mach. Learn.*, vol. 29, no. 2, pp. 131–163, 1997.

[41] J. Huang and C. X. Ling, "Using AUC and accuracy in evaluating learning algorithms," *IEEE Trans. Knowledge Data Eng.*, vol. 17, no. 3, pp. 299–310, Mar. 2005.